Representation of visual sequences in the tuning and topology of neuronal activity in the human hippocampus

Tibin John[1,2], Yajun Zhou[1], Ayman Aljishi[1,3], Bastian Rieck[5], Nicholas B. Turk-Browne[2,4], and Eyiyemisi C. Damisah[1,4,*]

[1]Department of Neurosurgery, Yale School of Medicine, New Haven, CT, USA
[2]Department of Psychology, Yale University, New Haven, CT, USA
[3]Department of Psychology, Vanderbilt University, Nashville, TN, USA
[4]Wu Tsai Institute, Yale University, New Haven, CT, USA
[5]Department of Computer Science, University of Fribourg, Fribourg, Switzerland
[*]Correspondence: eyiyemisi.damisah@yale.edu

SUMMARY

The hippocampus plays a critical role in the formation of memories and in the representation of time, yet the coding principles that connect these functions are poorly understood. We hypothesized that hippocampal neurons selective for specific visual stimuli adjust their tuning to encode sequence structure, smoothly combining sensory and temporal codes. In epilepsy patients who underwent intracranial EEG, we recorded neuronal activity from the hippocampus and control brain regions as they viewed looping sequences of visual scenes in structured (repeating) or random orders. The firing rates of hippocampal neurons to individual scenes were modulated by temporal distance from their preferred scene in structured sequences, increasing for nearby scenes and decreasing for distant scenes; this modulation was absent in random sequences and control regions. Analysis of population activity in local field potentials revealed that the looping sequence structure was embedded in a high-dimensional ring shape representing the serial order of the scenes. These findings show that human hippocampal neurons encode sequence structure in their representational geometry, extracting topological features of experience to add temporal continuity to sensory memories.

INTRODUCTION

The human brain uses multiple strategies to represent stimuli in memory, a process crucial for effective cognition and behavior. For example, imagine revisiting a friend's apartment without recalling the door number; seeing a unique doormat may help in identifying the correct door, but may leave some uncertainty. Fortunately, the time-based memory of reaching your friend's door after about ten seconds of walking from the elevator may help complete the recognition process successfully. This example illustrates how we can flexibly group stimuli in memory based on different attributes, including sensory similarity[1], spatial proximity[2], and temporal distance[3]. How does the brain combine sensory inputs with more abstract information from the sense of time, for which there is no sensory receptor?

Although the visual cortex processes sensory features from the current environment, higher-order systems are needed to incorporate regularities learned from past experiences in the same or similar environments. Initial studies in non-human primates demonstrated that extensive training on visual sequences of abstract fractals alters the tuning of neurons in inferior temporal cortex and perirhinal cortex such that their response to a fractal is proportional to the distance of that stimulus from their preferred fractal in the sequence[4]. Moreover, neurons in these regions encode pairs of fractals or objects that are presented together during paired associate learning[5] or

across saccadic eye movements[6]. More recent work in humans has shown that statistical learning of temporal pairs or graph communities in visual sequences increases the similarity of activity patterns evoked by the constituent stimuli in the hippocampus[7–9]. These findings suggest that the hippocampus is capable of learning long-range temporal regularities, pointing toward a role in elevating sensory representations into more abstract representations of sequence structure.

In this study, we test the hypothesis that the hippocampus encodes sequences in the tuning of neurons based on temporal distance from their initially preferred stimulus. Using intracranial recordings from patients with epilepsy, we examine the neuronal responses in the hippocampus and control regions to looping sequences of scene photographs with and without structure. Our results demonstrate that hippocampal neurons show increased firing to stimuli near to their preferred stimulus in a structured sequence and decreased firing to more distal stimuli in the sequence. We use topological data analysis to show that these changes at the level of individual neurons correspond to a population code for the global shape of the sequence, with local field potentials in the hippocampus embedding the looping structure as a high-dimensional ring in its representational space. This suggests a strategy in which the hippocampus combines its coding for sensory and temporal features to represent the geometry of experience in memory.

Revealing how sequence order modulates sensory coding contributes to a more comprehensive understanding of hippocampal function in the integration of content, time, and space. This has broad implications for understanding how we perceive and interact with the world, using consistent temporal regularities to shape the representation of sensory information at the neural level. This learning of sequence structure enables efficient prediction and behavior and could serve as the foundation of episodic memory.

RESULTS

We investigated how temporal regularities influence the tuning and population activity of neurons in the hippocampus of eight individuals (Figure 1a for microwire bundle locations; Supplementary Table 1 for subject demographics). These participants completed a passive viewing task in which they watched a stream of photographs of natural scenes in blocks of two conditions (Figure 1b). In the structured condition, 10 scenes were presented in a fixed order that wrapped around at the end, resulting in a looping circular sequence that repeated 15 times; the order was chosen randomly the first time (and fixed for subsequent repetitions) and thus was arbitrary in terms of the perceptual and semantic relationships between scenes. In the random condition, 10 other scenes were presented in a unique random order on each of the 15 repetitions (Figure 1c,d). Thus, the conditions were equated in the type, number, and frequency of stimuli, varying only in whether the order of the scenes was predictable.

Tuning of hippocampal neurons for natural scenes

Of the 144 single units we recorded (see Supplementary Figure 1 for spike-sorting metrics), 69 were in the hippocampus (HPC) and 75 were in non-hippocampal regions: 30 from the amygdala (AMY), 40 from the dorsal anterior cingulate cortex (dACC), and 5 from the anterior insula (AIN). We first quantified the initial selectivity of the firing of these units to individual scenes in both conditions. This served as a common baseline from which to assess changes in neuronal tuning attributable to sequence learning in the structured relative to random conditions. A neuron was identified with a preferred scene when the peak response to that scene during initial stream exposure (first 2 of 15 cycles) exceeded the 95th percentile of peak rates from surrogate tuning curves for that neuron created by 50,000 permutations of scene labels (Figure 1e,f). Among the

recorded units, 26 of 69 in the hippocampus (37%) and 21 of 75 in non-hippocampal regions (28%) were classified as selective (for an example selective hippocampal unit, see Figure 1f). The average firing rate of these neurons as a function of relative serial position (Figure 1g) indicates that their activity was selective to their preferred scene at baseline.

Changes in neuronal tuning with sequence learning

Having identified hippocampal neurons tuned to a preferred scene, we asked how exposure to a repeating sequence containing that scene would affect a neuron's tuning to other scenes in the sequence. To assess learning, we compared neuronal responses early in sequence exposure (first two repetitions) to late in sequence exposure (last repetition). We hypothesized that in the structured condition, neurons in the hippocampus would show increased responses to scenes that were nearby vs. far away from the preferred scene in the sequence. Indeed, hippocampal neurons showed significant modulation of firing rates based on the temporal distance from their preferred scene in the structured compared to random conditions(Figure 2a), responding more to the next scene (+1) in the sequence and less to the farthest scenes (+5/-5, +6/-4). This sequential modulation of tuning was even more striking when the data were folded across the distance = 0 axis to reflect absolute distance (Figure 2b). Heatmaps of firing rates across trials and scene distances also illustrated this dynamic modulation (Figure 2c). We summarized this effect for statistical analysis by calculating the slope of the early-to-late change in firing rate as a function of absolute distance from the preferred scene (Figure 2d; see Supplementary Figure 2 for forward and backward separately). In the structured condition, hippocampal units showed a significant negative slope (two-sided Wilcoxon signed-rank test, $p = 0.0012$), indicating that their tuning came to encode the sequence structure; this slope was more negative than in random condition (Mann-Whitney U test, $p = 0.0006$), which itself did not differ from chance ($p = 0.071$). Among the regions recorded, this effect was specific to the hippocampus, as non-hippocampal units did not show a negative slope in either the structured ($p = 0.79$) or random ($p = 0.73$) conditions or between the two conditions ($p = 0.87$).

Changes in representational similarity of population activity

We next asked whether this distance-dependent coding in single units scales up to the neural population level by analyzing local field potentials (LFPs). We converted the LFPs evoked by each scene to a time-frequency spectrogram, calculated the Pearson correlation between the spectrograms for all pairs of scenes from the same condition, and assessed how this representational similarity differed based on the sequence distance between the paired scenes (Figure 3a,b). In the hippocampus, the correlation between scene-specific LFP spectrograms changed from early to late sequence exposure in the structured condition in a distance-dependent manner (Figure 3c,d). Adjacent scenes in the sequence showed increased representational similarity over time (or *integration*), whereas distal scenes in the sequence (separated by a maximum of 5 scenes given the circular structure) showed decreased representational similarity over time (or *differentiation*) (Figure 3d,e). These integration and differentiation effects were responsible for a significant negative slope relating late minus early pair similarity to scene distance for the structured condition in the hippocampus (Figure 3f; two-sided Wilcoxon signed-rank test, $p = 0.0049$). This result was highly specific and not found for the random condition in the hippocampus ($p = 0.8460$) or in non-hippocampal regions for either the structured ($p = 1.0000$) or random ($p = 1.0000$) condition. The slope was more negative for structured than random in the hippocampus (Mann-Whitney U $p = 0.020$) but not in non-hippocampal regions ($p = 0.922$).

Emergence of ring structure in geometry of population activity

To examine whether the pairwise representational changes reflected a global reorganization of neural population codes, we used persistent homology from topological data analysis to quantify the geometric features of the arrangement of spectral LFP patterns in coding space. Persistent homology provides a data-driven, non-parametric measure of the shape of high-dimensional data (here, the time-frequency representations of each scene's LFP response) in terms of simplicial complexes. These complexes generalize graphs beyond capturing only pairwise interactions via edges by including multi-point faces, i.e., simplices, according to geometrical criteria like overlapping radii in the Vietoris–Rips filtration (Figure 4a-c). A collection of such simplices, i.e. a simplicial complex, can be analyzed for its topology at every possible radius, allowing analysis of connectivity structure across multiple scales. A characteristic shape of the data can then be extracted as the topological feature of simplicial complexes that persists across the most scales, evaluated using the persistence diagram[10,11]. We hypothesized that the most characteristic shape of scene representations late in exposure may be a topological loop or ring in the hippocampus mirroring the temporal circular structure of the looping sequence. To detect robust topological loops, we calculated persistence diagrams of Vietoris–Rips complexes to capture the shape of the data at multiple scales. 2-D hippocampal spectral LFP patterns in the structured condition showed a stable one-dimensional hole only in late exposure, indicative of a dispersion of visual representations into a circle from early to late exposure (Figure 4d). To quantify the prominence of the topological structure we employed the persistence gap metric, which measures how much the most persistent feature exceeds the next largest persistence (max persistence minus runner-up persistence; (Figure 4c). The persistence gap was compared to shuffled surrogate distributions of the low dimensional embeddings, which were used to form a null distribution for each condition (Figure 4e). This provided evidence that topological persistence emerged in the hippocampus for the structured condition (p = 0.0065) but not for the random condition (p = 0.19), nor in non-hippocampal regions for the structured (p = 0.13) or random (p = 0.51) conditions. Spatial statistics of point patterns using Ripley's H function (Figure 4f) also supported dispersion at intermediate distances in the hippocampus for structured (shuffled null distribution at r=0.5; p = 0.00640) but not random (shuffled null distribution at r=0.5; p = 0.99740) based on changes in Ripley's H function over inter-point distance r (Figure 4g) . Specifically, the hippocampus in the structured condition (red) shifted toward dispersion at intermediate distances, consistent with ring-like structure, whereas the random condition (pink) shifted towards clustering at intermediate distances, inconsistent with ring structure.

Angular coding of sequence position within ring structure

The topological analyses above demonstrate that hippocampal representations of the structured sequence are organized into a high-dimensional ring shape. However, this leaves open the question of where particular scenes fall on the ring. We hypothesized that their location would be ordered based on their serial position in the structured sequence. Plotting the scene representations in the space defined by the first two principal components of the evoked LFP spectrograms revealed that scenes formed a trajectory corresponding to their order in the sequence during late exposure to the structured sequence (Figure 5a,b). Namely, there was a relationship between angle along the best-fit ellipse and structured sequence order in the hippocampus, which was not observed for the random condition or outside the hippocampus (Figure 5c). Comparisons with scene-shuffled surrogate data confirmed that the observed decrease in circular-linear regression error was significant. Indeed, only the hippocampus structured condition show a significant improvement in the angle-scene order mapping over time (p = 0.017; observed change = -0.51 rad), representing a refinement of a directional, ring-like code for temporally structured

stimuli. In contrast, the hippocampus random condition (p = 0.55; observed change = 0.03 rad) and non-hippocampal structured (p = 0.22; observed change = -0.14 rad) and random (p = 0.67; observed change = 0.10 rad) conditions did not show such improvement (Figure 5d). Thus, sequence information is encoded in the hippocampus at the level of individual neurons, pairs of LFP patterns, the geometry of the global embedding of these patterns, and trajectories along that geometric representation.

Emergence of rhythmic activity with sequence learning

To explore potential mechanisms underlying the conversion of sequenced inputs into geometric representations, we analyzed oscillatory patterns associated with exposure to temporal structure. A 4 Hz rhythm emerged in LFP power spectra (Figure 6a,b) in the hippocampus from early to late exposure in the structured condition relative to random condition in the hippocampus (Mann-Whitney U, p = 0.00000096) but not outside the hippocampus (p = 0.74). Moreover, spike train power spectral analysis revealed a selective increase in rhythmicity at 4 Hz in the hippocampus during the structured relative to random condition with a peak frequency at 4.4 Hz (p = 0.00020, red dots (Figure 6c), suggesting engagement of temporal encoding mechanisms. Outside the hippocampus there was no such increase in oscillatory power, instead showing a decrease at peak frequency 8.9 Hz, p = 0.03314). These structure-specific theta rhythmic changes in LFP and single unit spiking were not independent but temporally coupled, as hippocampal units also showed an increase in spike-field coherence from early to late exposure in the structured condition (Figure 6d). The average change in coherence in 1-4 Hz was significantly greater than 0 among hippocampus units during the structured condition (Wilcoxon signed-rank test; p = 0.0016) but not the random condition (p = 0.28) or among non-hippocampal units in the structured (p = 1.00) or random (p = 0.88) conditions. Finally, we observed a change in circular-linear correlation from early to late trials calculated relative to shuffled null distributions for the structured condition in the hippocampus (early r = 0.817, late r = -0.945; p = 0.00076), which was not seen in the random condition (early r = -0.711, late r = -0.049; p = 0.18). (Figure 6e,f) This suggests that hippocampal neurons may adjust the timing of their firing within subsecond oscillations to reflect the sequence.

DISCUSSION

Our findings demonstrate that arbitrary visual sequences can reshape the geometry of sensory codes in human hippocampal neurons, rather than being kept separate in different 'what' and 'when' streams[12]. Initially, many hippocampal neurons responded selectively to individual stimuli, providing a stable baseline representation[13–15]. With repeated exposures to temporally structured sequences, these selective responses evolved: the tuning integrated scenes close in time and differentiated scenes that were farther apart. Importantly, the sensory inputs themselves were fixed, demonstrating that these changes reflect learning of the sequence of inputs. Thus, the hippocampus smoothly incorporates sequence structure into its code for stimulus identity.

Crucially, we used topological data analysis[10,11] and spatial statistics[16] to reveal a global, manifold-level reorganization of hippocampal representations. For structured sequences, scene-evoked neural activity exhibited a stable ring-like topology — a low-dimensional "hole" preserving temporal order and structure. Such a persistent topological feature did not arise under random sequences or in non-hippocampal regions, underscoring the unique potential of the hippocampus to map temporal structure onto a distance-dependent manifold. Spatial point pattern analyses (Ripley's H function) further supported this ring-like shape, highlighting the role of the hip-

pocampus in forming a coherent geometric code that integrates temporal information beyond local pairwise relationships.

Recent work has shown that hippocampal neurons respond to probabilistic transitions between stimuli[9] and extract the temporal structure of visual experience. Our findings build on this work by demonstrating that learning within hippocampal cells involves not only near integration, as shown before, but also far differentiation. Notably, near integration and far differentiation did not occur when participants were shown random sequences that were otherwise matched and did not occur reliably outside of the hippocampus. Furthermore, using persistent homology to examine global structure, we additionally show that learning reshapes the representational geometry of the hippocampus, enabling it to encode the sequence structure of cyclical experiences.

Distance-dependent changes in neuronal tuning and representational similarity could result from known plasticity mechanisms. According to the nonmonotonic plasticity hypothesis (NMPH)[17], the neighboring scene that follows a neuron's preferred scene in the structured sequence may be integrated into the neuron's tuning because the response to the preferred scene persists into the perception of the next scene, leading to robust coactivation that promotes synaptic strengthening. In contrast, the preferred scene may be less active during the perception of more distant scenes in the structured sequence, leading to moderate coactivation that promotes synapting weakening. Behavioral time-scale plasticity (BTSP)[18] and theta sequences[19,20] may additionally contribute, enabling synaptic changes over behavioral timescales and providing temporal compression of event sequences.

The emergence of 4 Hz rhythmicity particularly in hippocampal spiking and LFP patterns during structured sequences is reminiscent of the theta rhythm in navigating rodents[21,22]. This population dynamic may enhance the binding of temporally proximal stimuli and support the retrieval of sequential information using the theta rhythm as a population-level reference clock[23,24]. More generally, our results may reflect the development of attractor dynamics within the hippocampus, where local excitation and long-range inhibition produce stable activity "bumps" along a time dimension[25,26]. Such attractor networks could maintain a stable temporal code, reinforcing connections between temporally adjacent stimuli and segregating distant ones in a way that reflects the geometry of their temporal relationships.

Our results also extend the notion of "concept cells" in the hippocampus — which can encode abstract, multimodal features[27,28] — by showing that individual cells can also encode sequences of visual stimuli to form flexible memory representations of dynamic environments. Neurons adapt their tuning to reflect temporal relationships, aligning with theories that the hippocampus forms conjunctive representations that bind multiple aspects of experience[29,30]. By encoding both what and when, these cells may support episodic memory functions in the hippocampus, which require associating events in sequence.

Our approach provides a testbed for investigating temporal sequence coding in the human hippocampus at the level of single neurons and neural populations[31]. Understanding how sequence tuning and geometric representations emerge and are maintained is critical for deciphering the neural basis of temporal cognition and episodic memory. Disruptions in such coding may contribute to memory deficits in conditions like Alzheimer's disease[32–34].

METHODS

Study participants

Eight participants (3 males and 5 females, 6 right-handed and 2 left-handed, ages 17 to 61 years) with medication-refractory epilepsy undergoing intracranial EEG electrode implantation for seizure localization were enrolled in the study after providing informed consent (see Supplementary Table 1 for subject demographics). Electrode planning and implantation was made exclusively for clinical purposes. Behnke-Fried depth electrodes (Ad-Tech Medical Instrument Corp., Oak Creek, WI, USA) with 40uM microwires extending from the tip were used to record single units from the hippocampus (HPC), amygdala (AMY), anterior insula (AIC), and dorsal anterior cingulate cortex (dACC) (Fig 1a, supplementary Fig 1 and supplementary Tables 1 and 2). All subjects remained on their home antiseizure medications for the duration of the study. The study was approved by the Institutional Review Board at Yale University.

Task design

Participants were exposed to sequences of visual scenes while neural activity was recorded. Visual stimuli consisted of 20 photographs of natural scenes, based on the importance of the human hippocampus for scene perception[35]. Two types of sequences were constructed: in the structured condition, 10 of the scenes were selected to form a fixed sequence that repeated in the same order 15 times (looping); in the random condition, the remaining 10 scenes were also presented in each of the 15 repetitions, but their order was randomized on each repetition. Each scene was displayed for 1 s, followed by a fixation cross for 1 s (Fig 1b, c). The order of the conditions was counterbalanced among the eight participants to prevent order effects.

Electrophysiological recording

Voltage traces were high-pass filtered at 300 Hz for spike detection. Spikes were then sorted offline with Waveclus[36]. Sorting parameters were calibrated per participant to account for variability in signal amplitude and background noise. Putative single units were retained if they showed stable waveforms, had fewer than 3% of spikes with inter-spike intervals under 3 ms, and met minimum firing rate thresholds. We thus identified a total of 69 single units in the hippocampus and 75 in non-hippocampal regions (Supplementary Fig 1).

Single-unit analysis

We aligned spike times to scene onset (time 0) and calculated firing rates within a 1000 ms post-stimulus window, subtracting a 1000 ms pre-stimulus baseline. Each unit's firing rate profile was averaged across trials. A unit was deemed "scene-selective" if its maximum firing for any scene exceeded the 95th percentile of a shuffle distribution generated by 50,000 random permutations of scene labels. The scene evoking the highest mean firing rate in the early trials (i.e. the average of trials 1 and 2) was designated as the preferred scene for that unit. Firing rates in early versus late trials (i.e., last trial) were compared across structured and random conditions to assess how repeated exposure modulated selectivity. The hippocampal and nonhippocampal units were analyzed separately (Fig. 1e-g).

Distance-dependent analysis

To examine how firing rates varied with temporal distance from the preferred scene, we computed, for each scene, its position relative to the preferred scene in the sequence. In the structured condition, distance followed the fixed circular order; in the random condition, distance was determined by time regardless of each random permutation. A linear slope of firing rate by distance was calculated for each unit in early (i.e., average of trials 1 and 2) and late exposure periods (i.e., last trial), and the reliability of the change in slope across participants was evaluated with Wilcoxon signed rank and Mann-Whitney U tests for comparisons to 0 within condition and between conditions, respectively (Fig 2a - d).

Local field potential analysis

LFP signals from microwires (or macro contacts when unavailable in Subjects 1 and 2) were downsampled to 2000 Hz. Time-frequency representations were computed after a short-time Fourier transform over a 600 ms window starting at scene onset, normalized by the pre-onset baseline spectrum during the fixation cross and expressed in decibels (Fig 3a). The resulting spectrograms were averaged for each scene to determine a unique LFP scene code in the early phase (first 7 trials) vs late phase (last 7 trials) which were subsequently analyzed for changes in the structure of the resulting point clouds (Fig 4d). This change in trial number is due to the variability in LFP data and lower SNR ratio compared to single units. For oscillatory analyses, the early phase spectrograms were averaged within each session and subtracted from the late phase spectrograms for each condition; total power in the 3-6 Hz band was extracted from these difference spectrograms to measure the change in theta rhythm power (Fig 6a). Paired Wilcoxon tests were performed to evaluate the significance of relative changes in this frequency band between structured and random conditions and each brain region (Fig 3f, 6b). Spike-field coherence was also evaluated in these same time windows with the scipy.signal coherence method on aligned selective unit spike trains with at least 150 spikes and LFP signals in the 1–50 Hz range to detect frequency bands where these signals became coupled (Fig 6c, d). Change in total power in the 1-4 Hz band were compared to 0 using a two-sided Wilcoxon signed rank test in each condition and brain region.

Dimensionality-reduced LFP pattern analysis

To capture higher-level structure in LFP patterns, we concatenated spectral features across channels for each scene. After z-scoring, we applied principal component analysis (PCA) to all evoked LFP spectrograms across scenes within the early and late trials to reduce dimensionality respectively (Fig 3 Fig 5). Scene-by-scene correlation matrices were generated for early and late trials and the difference was compared across different conditions (structured vs random) and regions (hippocampus and non hippocampus)(Fig 3). The top 6 PCs were then embedded in 2-D space using Isomap to visualize how scenes clustered during early versus late exposure of structured versus random conditions (Fig 4). The best fit ellipse of the dimensionality reduced LFP spectrograms were then computed during early vs late trials and circular linear correlation of angle with scene order was computed (Fig 5). Permutation tests assessed whether changes from early to late exceeded chance levels

Topological data analysis

Topological data analysis (TDA) is a nascent field, drawing upon concepts from computational topology to describe the "shape" of data at multiple scales. One of the most general and prominent TDA techniques is *persistent homology*. Given a dataset, persistent homology first calculates a topological approximation of the data. Such an approximation typically takes the form of a simplicial complex, which is a data structure that generalizes a graph beyond dyadic interactions by incorporating higher-order relations (simplices) between three or more elements. Here, we used a Vietoris–Rips complex, which is a simplicial complex consisting of progressively more fine-grained representations of a dataset. This construction is followed by the calculation of topological shape features like connected components, cycles, and voids, which are ultimately represented in a compact 2-D representation — the persistence diagram. A point (x, y) in a persistence diagram denotes a topological feature being "born" at scale x and "destroyed" at scale y. Despite its low dimensionality, this representation is expressive and provably stable to noise in the data. Moreover, persistence diagrams permit filtering the original data based on the idea of discerning between signal and noise, which was shown to be particularly relevant in the context of data analysis[11].

Persistent homology of scene representations

We performed persistent homology analyses on the high-dimensional LFP spectrograms to assess the emergence of a ring-like (one-dimensional hole) structure in the hippocampus (Fig 4d). Specifically, we used Ripser to compute Vietoris–Rips complexes and generate persistence diagrams capturing 0-D and 1-D topological features. The first Betti number (β_1)identifies loops in the data. We quantified their prominence relative to less stable topological features with a *persistence gap*, defined as the difference between the max persistence and the second-largest persistence[10,11]. Shuffled surrogate distributions of scene labels or dimensional embeddings were used to form a null distribution for each condition. We then tested whether hippocampus in the structured condition exhibited a significantly larger gap shift than the random condition or either condition in the non-hippocampus data.

Spatial statistics of representation changes (Ripley's H)

To examine whether the 2-D embeddings of the evoked LFP spectrograms in isomap space showed ring-like dispersion, we computed Ripley's H function, which measures how points (here, representing individual scenes) deviate from complete spatial randomness at various radii (Fig 4f,g). Values of H(r)$>$0 suggest clustering at distance r, whereas H(r)$<$0 indicates dispersion. We calculated H(r) for embeddings from early and late exposure, then compared the structured condition to the random condition in both hippocampus and non-hippocampus. A negative shift in H(r) at intermediate distances may indicate the formation of a ring-like manifold with a gap around the circle. We assessed significance by comparing observed changes to a label-shuffled or scene-shuffled baseline.

Theta phase coding analysis

We examined spike-LFP phase relationships (Fig 6e, f) in the 3.5–9.5 Hz band using the Hilbert transform to extract instantaneous phase. Spike times were aligned to the corresponding LFP phase, and each unit's data were grouped into early versus late exposure. We plotted phase-time heatmaps and computed circular-linear correlations to test whether the hippocampus displayed

stronger phase coding over time. Surrogate tests were performed by shuffling scene labels or adding random jitter to spike times (uniform random from +/- 500 milliseconds) to generate null distributions, and we compared the real data's correlation changes to these nulls.

RESOURCE AVAILABILITY

Lead contact

Requests for further information and resources should be directed to and will be fulfilled by the lead contact, Eyiyemisi C Damisah (eyiyemisi.damisah@yale.edu).

Materials availability

This study did not generate new materials.

Data and code availability

All analyses were conducted using Python (version 3.9.16) with libraries including NumPy, Pandas, SciPy, Matplotlib, and scikit-learn. The data generated in this study are freely available without stipulation or restrictions and can be obtained by request to the corresponding author via email. All original code has been deposited at (Hippocampal Sequences repository) and is publicly available as of the date of publication. Any additional information required to reanalyze the data reported in this paper is available from the lead contact upon request.

ACKNOWLEDGMENTS

The authors thank the members of the Yale Comprehensive Epilepsy Center for excellent patient care and the patients who participated in this study. This work was funded by a Hypothesis Fund seed grant.

AUTHOR CONTRIBUTIONS

Conceptualization, E.C.D., and N.T.B; methodology, A.A., T.B., E.C.D., and N.T.B; investigation, T.B., A.A., Y.Z., B.R., N.T.B., and E.C.D.; writing-–original draft, T.B.; writing-–review & editing, T.B., E.C.D., B.R., and N.T.B.; funding acquisition, E.C.D.; resources, E.C.D., and N.T.B.; supervision, B.R., E.C.D., and N.T.B.

DECLARATION OF INTERESTS

The authors declare no competing interests

MAIN FIGURE TITLES AND LEGENDS

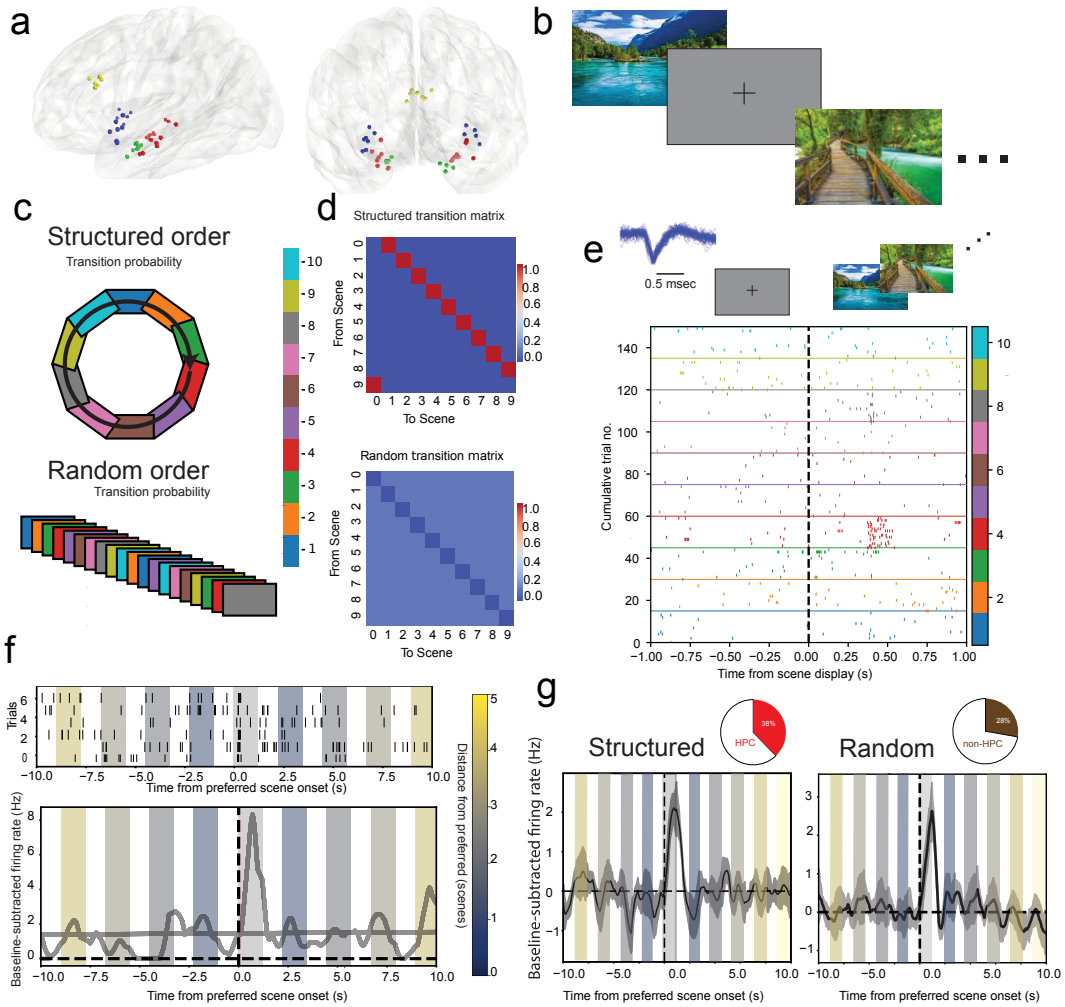

Figure 1: Hippocampal neurons exhibit selective firing to individual visual scenes during initial sequence exposure. (a) 3-D brain reconstructions from eight patients displaying the electrodes color-coded by brain region: hippocampus (red), amygdala (green), insula (blue), and dorsal anterior cingulate cortex (yellow). (b) Participants viewed a stream of 10 distinct scene images, displayed for 1 s followed by 1 s of fixation. In the structured condition, the order of scenes was fixed and repeated 15 times continuously, resulting in a circular sequence. In the random condition, the order of the scenes was randomized on each of the 15 repetitions eliminating sequential structure. (c) The identities of the scenes are color-coded (1–10) and (d) the transition probabilities are indicated in scene-by-scene matrices. (e) Top: Representative spike waveform of a HPC neuron. Bottom: Raster plot of this neuron's spiking activity (indicated with dots). Each row is a trial and the 15 trials for each of the 10 scenes are grouped in adjacent rows. The x-axis is aligned to scene onset (time 0, dashed line), revealing that this unit fires selectively to a preferred scene (#4, red). (f) Example conversion of spike rasters to firing rates over time, showing heightened responses during the preferred scene's time window.(g) Pie charts: Approximately 38% of HPC units (26/69) and 28% of non-HPC units (21/75) showed preferential responses to one scene during initial exposure (first two repetitions). Bottom: Mean baseline-subtracted firing rates for initial exposure in structured (left) and random (right) conditions. Shaded areas represent SEM and the color gradient reflects temporal distance from the preferred scene.

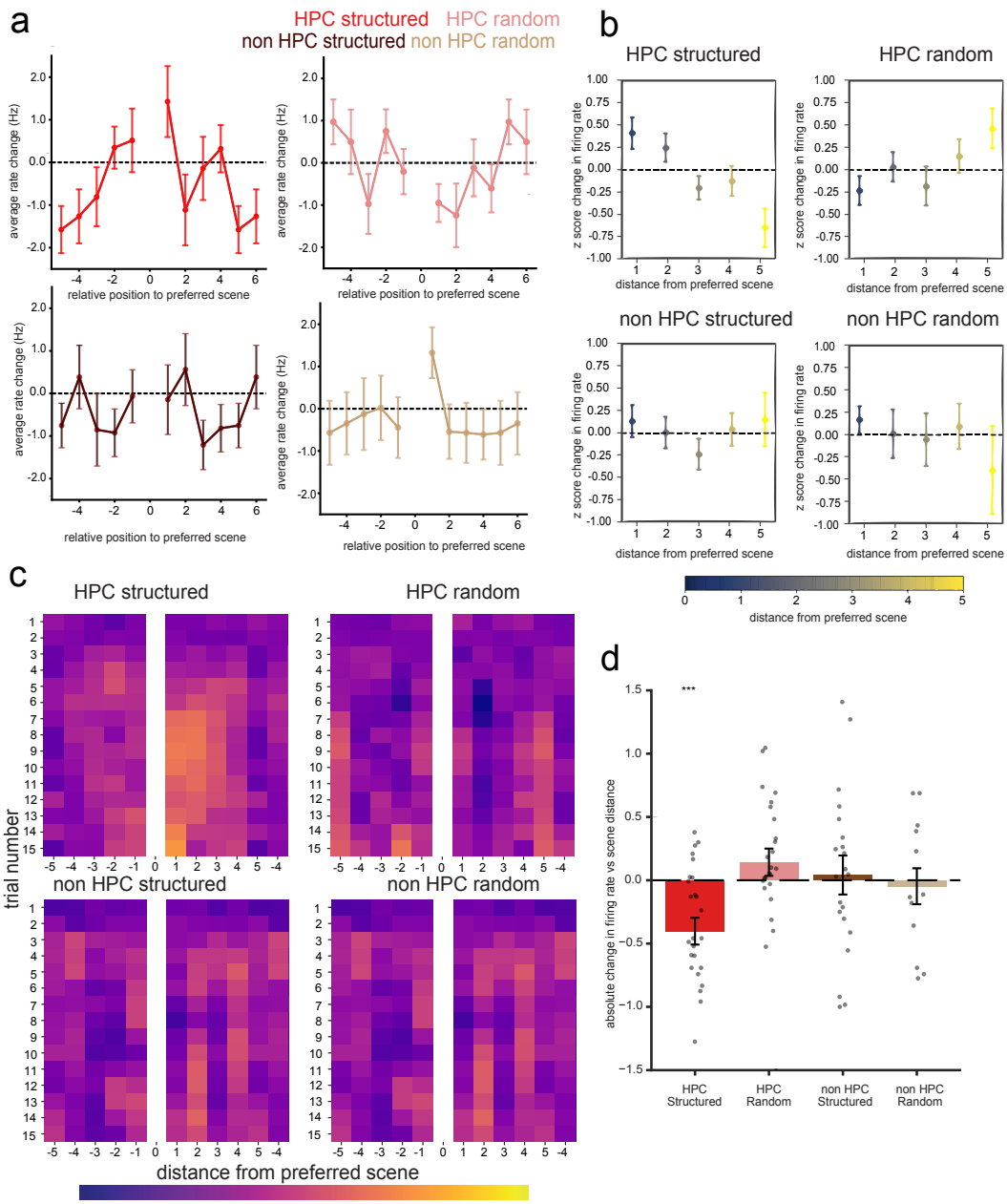

Figure 2: Hippocampal neurons encode sequence structure in firing rate changes. (a) Average firing rate changes of HPC(top) and non-HPC (bottom) neurons from early to late exposure as a function of each scene's relative distance from a neuron's preferred scene in structured (left) and random (right) conditions. (b) Each dot represents the change in the slope of the distance-dependence of firing for a single unit (defined as slope of the best fit regression line to firing rate vs absolute scene distance) from 1st two trials to last trial. Bars represent the mean across units within region and condition, with HPC units showing a more negative slope in structured than random conditions. The change in slope was also lower than zero only in HPC units during the structured condition (two-sided Wilcoxon-signed rank test). Units in non-HPC regions showed no significant difference from zero or between conditions. (c) Evolution of scene firing rates visualized as heatmaps. Rows correspond to trials and columns correspond to distance from the preferred scene. Warmer colors indicate higher firing rates. (d) Average change in firing rates (z-scored within each unit) as a function of the absolute distance from the preferred scene (x-axis and colors) for HPC (top) and non-HPC (bottom) units in structured (left) and random (right) conditions. Error bars represent SEM. *** $p < 0.001$.

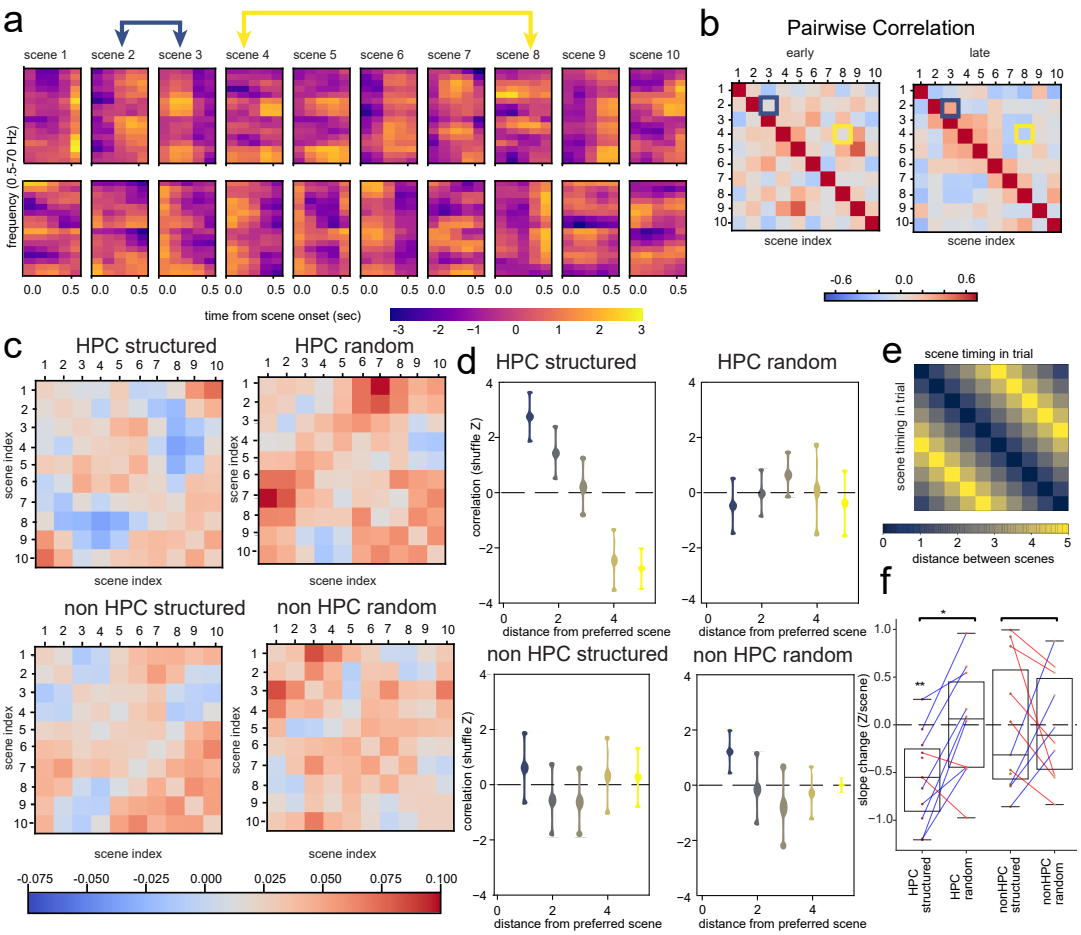

Figure 3: The hippocampus encodes sequence structure in the representational similarity of population activity. (a) Average spectrogram of LFP power aligned to the onset of each scene, for early (top) and late (bottom) sequence exposure. (b) Example scene-by-scene correlation matrix for early and late exposure. Distance between scenes is illustrated with arrows around the spectrograms and in matrix form, with adjacent scenes in navy and distal scenes in yellow. (c) Group-level changes in scene-to-scene correlations (late minus early), with warm colors indicating increased representational similarity over time and cool colors indicating decreased representational similarity over time. (d) Average z-scored changes in representational similarity normalized to a scene-label shuffled distribution of differences between early and late exposure as a function of sequence distance (indicated on x-axis and by color code). Error bars represent SEM. (e) Color-coded distance matrix key for (b, c) showing nearby scenes in navy and distal scenes in yellow. (f) Box plot of slope changes in LFP correlation vs. scene distance for individual sessions in the HPC or non-HPC regions for structured and random conditions. Horizontal lines in each box denote the median, edges represent the 25th and 75th percentiles, and whiskers extend to 1.5x the interquartile range. Each session appears as a single point; lines connect the same session across structured and random conditions, with blue lines indicating higher magnitude slopes for structured sequences and red lines indicating higher magnitude slopes for random sequences. * $p < 0.05$, ** $p < 0.01$.

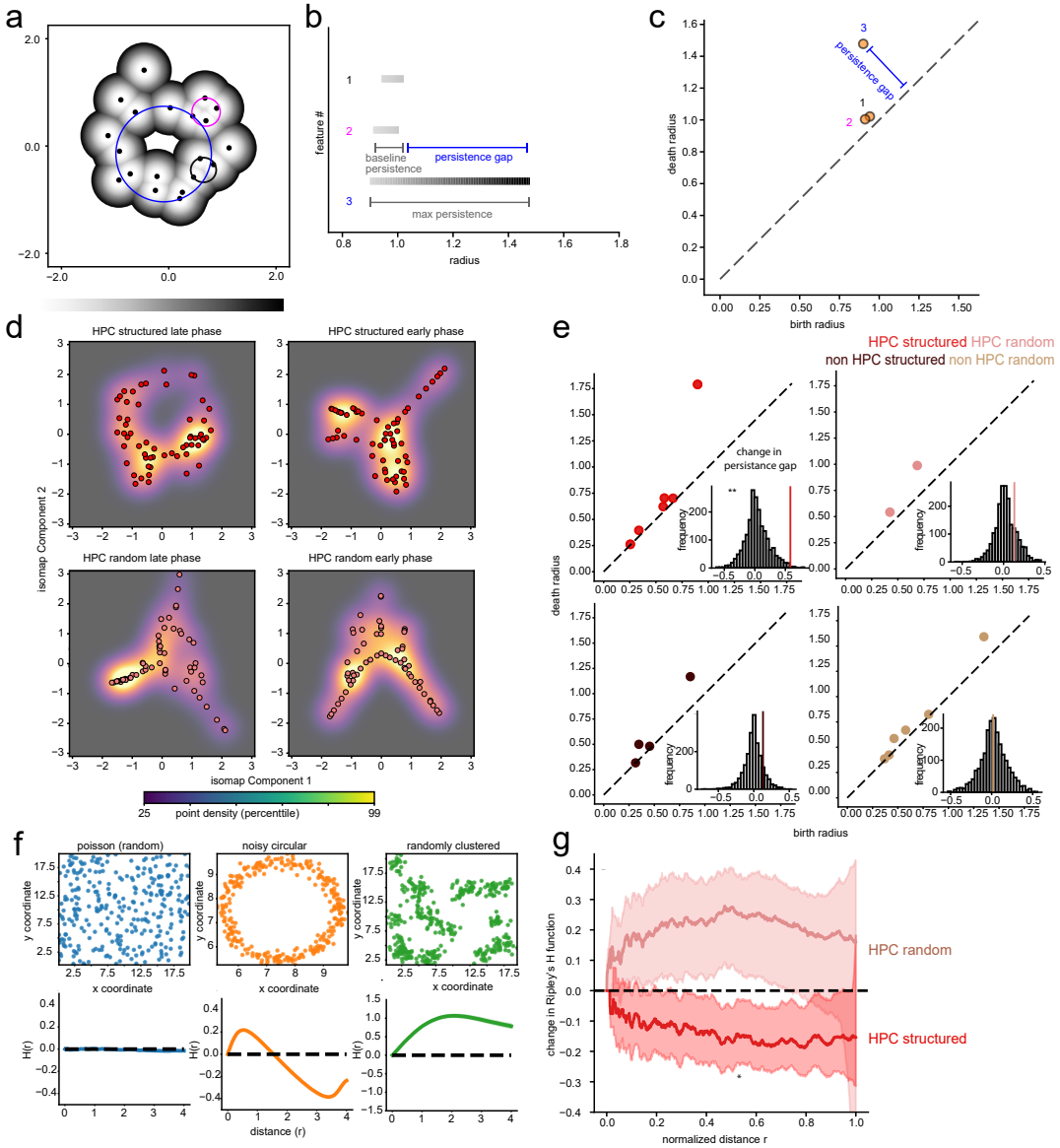

Figure 4: Emergence of a ring-like topological structure in hippocampal population activity. (a) Schematic illustrating how persistent homology captures the shape of a high-dimensional point cloud of LFP spectral patterns. As the connectivity radius (grayscale bar) grows, individual data points become linked into simplices. Topological features (e.g., loops) appear ("birth") and vanish ("death"), as summarized by persistence diagrams (b, c). Three hypothetical features shown (labeled 1–3), with each feature's lifespan measured from birth radius (x-axis) to death radius (y-axis). The persistence gap (blue horizontal bar) reflects how stably a loop persists, computed as the difference between its maximum and runner-up persistence. (d) 2-D embeddings (using PCA + Isomap) of HPC LFP patterns during structured (top) vs. random (bottom) conditions. Circles indicate single scene exposures, colored by local density (cool = low, hot = high). Comparing late (left) and early (right) exposure reveals that HPC population activity organizes into a ring-like manifold over time in the structured condition. In contrast, late exposure in the random condition (bottom) shows no clear emergence of ring structure. (e) Persistence diagrams (birth vs. death radius) and inset histograms for persistence gap metric by region and condition. The dashed diagonal line indicates where a feature's birth and death coincide (i.e., zero persistence). (f) Schematic illustrating how spatial distributions of points map onto Ripley's H function. Simulated data (top) and corresponding H functions (below) for three example patterns: Poisson-like (random, left), noisy circle (middle), and randomly clustered (right). H values above zero indicate clustering at a given distance, while values below zero indicate dispersion. (g) Line plots show the mean with 95% CI of changes in Ripley's H function over distance r for HPC in random (pink) vs. structured (red) conditions. * $p < 0.05$, ** $p < 0.01$.

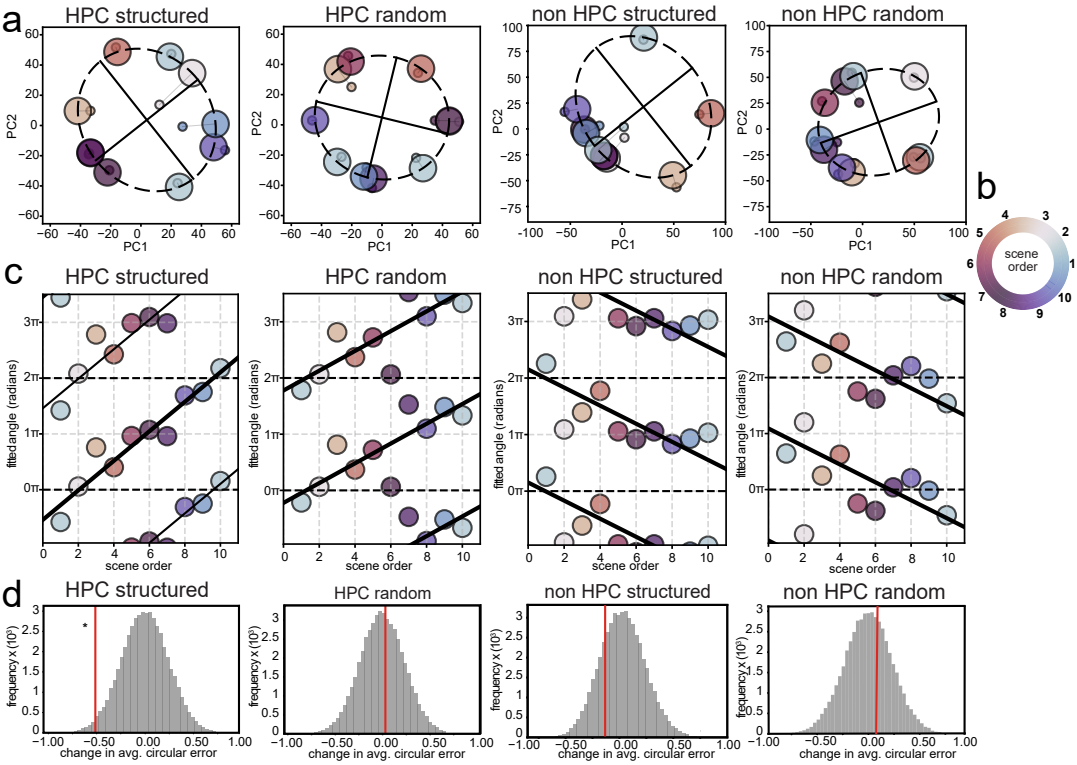

Figure 5: Hippocampal scene representations form a directional ring-like trajectory reflecting sequence order. (a) Projections of scene-evoked LFP representations late in exposure onto the first two principal components (PC1 and PC2) for HPC and non-HPC regions under structured and random conditions. Each point corresponds to the channel-concatenated representation of a single scene. Dashed ellipses represent best-fit ellipses to the scene clusters. Transparent points indicate points prior to projection onto best-fit ellipse. In the HPC, scenes in the structured condition form a ring-like arrangement with angle closely tracking their order in the sequence. This organized mapping is weaker or absent in the random condition for HPC and in both conditions for non-HPC regions. (b) Color-coded key by scene order from 1 to 10. (c) Circular-linear regression showing the angle around the best-fit ellipse (y-axis) against scene order (x-axis). Each dot represents a scene, and lines indicate the best-fit regression. In the HPC, the angle-scene order relationship is coherent for the structured condition, with a directional ordering of scenes along the ellipse. (d) Distributions of differences in circular-linear regression error (late minus early exposure) computed from scene-shuffled surrogate data for each condition. The red dashed line indicates the observed difference * $p < 0.05$.

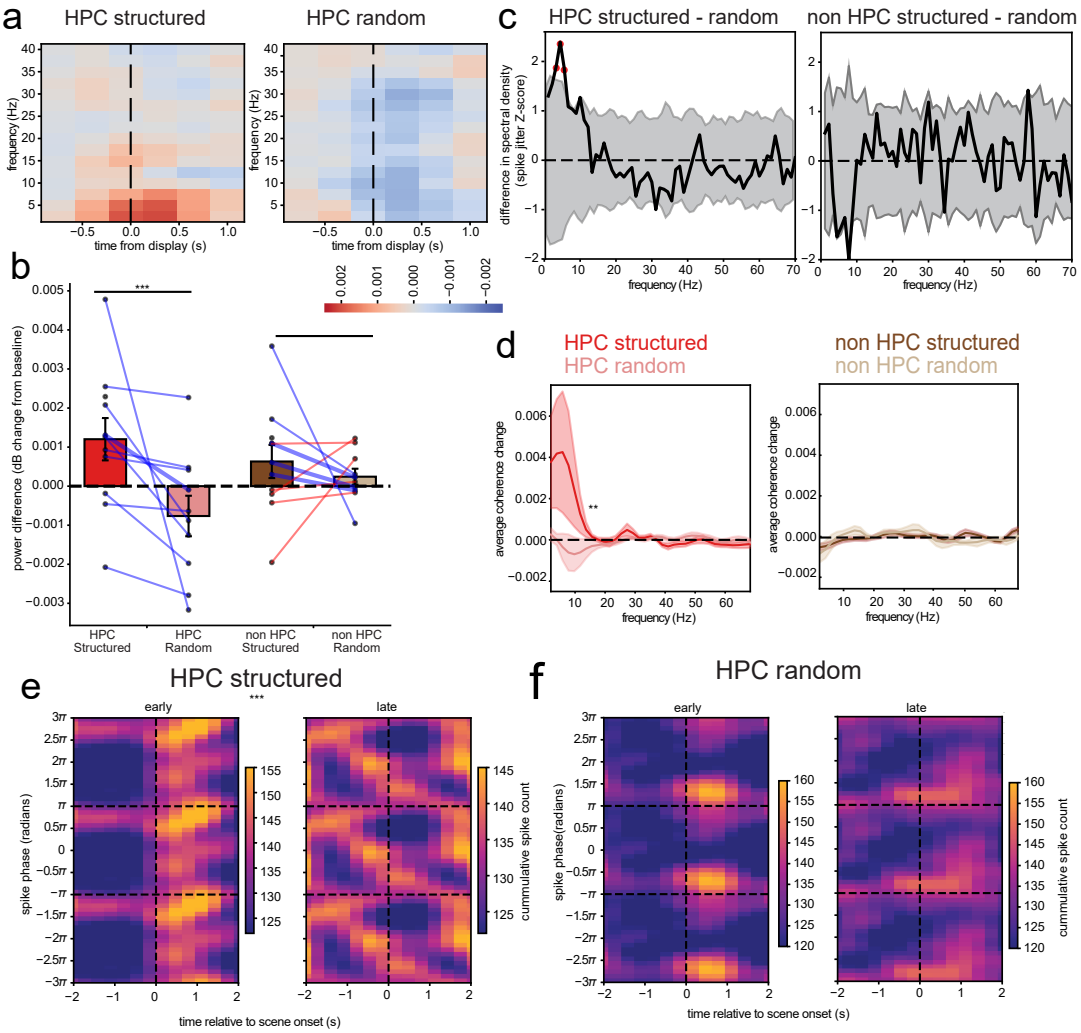

Figure 6: Emergence of rhythmic and phase coding during structured sequences. (a) Heatmaps showing the difference in power spectra between late and early exposure in the structured condition (left) and random condition (right) for HPC. Frequency is on the y-axis; time is on the x-axis; color indicates power change. (b) Bar plot representing the change in power at 4 Hz; error bars indicate SEM. (c) Difference in spike train power spectra for HPC compared to spike jittered null model showing the difference between late and early exposure under each condition. Shaded areas indicate SEM; red dots highlights the change at 4 Hz. (d) Average spike-field coherence change between early and late exposure for HPC (left) and non-HPC (right). (e) Phase spectrogram representing the theta phase relationship of spikes (3.5–9.5 Hz) relative to preferred scene onset for hippocampal units in the structured condition and (f) random condition. Heatmaps show spike-phase coupling over time from -1 to 1 second relative to scene onset; color represents spike counts ** $p < 0.01$, *** $p < 0.001$

References

1. Rogers, T.T., and McClelland, J.L. (2004). Semantic Cognition: A Parallel Distributed Processing Approach. Cambridge, MA: MIT Press.

2. Mishkin, M., Ungerleider, L.G., and Macko, K.A. (1983). Object vision and spatial vision: two cortical pathways. Trends in Neurosciences *6*, 414–417.

3. Howard, M.W., and Eichenbaum, H. (2013). The hippocampus, time, and memory across scales. Journal of Experimental Psychology: General *142*, 1211–1230.

4. Miyashita, Y. (1988). Neuronal correlate of visual associative long-term memory in the primate temporal cortex. Nature *335*, 817–820.

5. Sakai, K., and Miyashita, Y. (1991). Neural organization for the long-term memory of paired associates. Nature *354*, 152–155.

6. Li, N., and DiCarlo, J.J. (2008). Unsupervised natural experience rapidly alters invariant object representation in visual cortex. science *321*, 1502–1507.

7. Schapiro, A.C., Kustner, L.V., and Turk-Browne, N.B. (2012). Shaping of object representations in the human medial temporal lobe based on temporal regularities. Current Biology *22*, 1622–1627.

8. Schapiro, A.C., Turk-Browne, N.B., Norman, K.A., and Botvinick, M.M. (2016). Statistical learning of temporal community structure in the hippocampus. Hippocampus *26*, 3–8.

9. Tacikowski, P., Kalender, G., Ciliberti, D., and Fried, I. (2024). Human hippocampal and entorhinal neurons encode the temporal structure of experience. Nature *635*, 160 –167.

10. Rieck, B., and Leitte, H. (2017). Agreement analysis of quality measures for dimensionality reduction. In Topological Methods in Data Analysis and Visualization IV: Theory, Algorithms, and Applications VI. Springer pp. 103–117.

11. Hensel, F., Moor, M., and Rieck, B. (2021). A survey of topological machine learning methods. Frontiers in Artificial Intelligence *4*, 681108.

12. Hebart, M.N., and Hesselmann, G. (2012). What visual information is processed in the human dorsal stream? Journal of Neuroscience *32*, 8107–8109.

13. Quiroga, R.Q., Reddy, L., Kreiman, G., Koch, C., and Fried, I. (2005). Invariant visual representation by single neurons in the human brain. Nature *435*, 1102–1107.

14. Hodgetts, C., Shine, J., Lawrence, A., Downing, P., and Graham, K. (2016). Evidencing a place for the hippocampus within the core scene processing network. Human brain mapping *37*, 3779–3794.

15. Lee, S.M., Shin, J., and Lee, I. (2023). Significance of visual scene-based learning in the hippocampal systems across mammalian species. Hippocampus *33*, 505–521.

16. Jafari Mamaghani, M., Andersson, M., and Krieger, P. (2010). Spatial point pattern analysis of neurons using ripley's k-function in 3d. Frontiers in neuroinformatics *4*, 1285.

17. Ritvo, V.J., Turk-Browne, N.B., and Norman, K.A. (2019). Nonmonotonic plasticity: how memory retrieval drives learning. Trends in Cognitive Sciences *23*, 726–742.

18. Bittner, K.C., Milstein, A.D., Grienberger, C., Romani, S., and Magee, J.C. (2017). Behavioral time scale synaptic plasticity underlies ca1 place fields. Science *357*, 1033–1036.

19. Skaggs, W.E., McNaughton, B.L., Wilson, M.A., and Barnes, C.A. (1996). Theta phase precession in hippocampal neuronal populations and the compression of temporal sequences. Hippocampus *6*, 149–172.

20. Foster, D.J., and Wilson, M.A. (2006). Reverse replay of behavioural sequences in hippocampal place cells during the awake state. Nature *440*, 680–683.

21. Lever, C., Kaplan, R., and Burgess, N. (2014). The function of oscillations in the hippocampal formation. Space, time and memory in the hippocampal formation pp. 303–350.

22. Buzsáki, G. (2006). Rhythms of the Brain. Oxford University Press.

23. Vivekananda, U., Bush, D., Bisby, J.A., Baxendale, S., Rodionov, R., Diehl, B., Chowdhury, F.A., McEvoy, A.W., Miserocchi, A., Walker, M.C. et al. (2021). Theta power and theta-gamma coupling support long-term spatial memory retrieval. Hippocampus *31*, 213–220.

24. Lisman, J.E., and Jensen, O. (2013). The theta-gamma neural code. Neuron *77*, 1002–1016.

25. Tsodyks, M.V., and Sejnowski, T.J. (1995). Rapid state switching in balanced cortical network models. Network: Computation in Neural Systems *6*, 111–124.

26. Knierim, J.J., and Zhang, K. (2012). Attractor dynamics of spatially correlated neural activity in the limbic system. Annual Review of Neuroscience *35*, 267–285.

27. Quiroga, R.Q., Reddy, L., Kreiman, G., Koch, C., and Fried, I. (2005). Invariant visual representation by single neurons in the human brain. Nature *435*, 1102–1107.

28. Quiroga, R.Q. (2012). Concept cells: the building blocks of declarative memory functions. Nature Reviews Neuroscience *13*, 587–597.

29. Alexander, A.S., Robinson, J.C., Dannenberg, H., Kinsky, N.R., Levy, S.J., Mau, W., Chapman, G.W., Sullivan, D.W., and Hasselmo, M.E. (2020). Neurophysiological coding of space and time in the hippocampus, entorhinal cortex, and retrosplenial cortex. Brain and Neuroscience Advances *4*, 2398212820972871.

30. Eichenbaum, H. (2014). Time cells in the hippocampus: a new dimension for mapping memories. Nature Reviews Neuroscience *15*, 732–744.

31. Rutishauser, U., Jadhav, S.P., and Frank, L.M. (2021). The architecture of human memory: Insights from human single-neuron recordings. Journal of Neuroscience *41*, 883–890.

32. Park, J.H., and Lee, S.A. (2021). The fragility of temporal memory in alzheimer's disease. Journal of Alzheimer's Disease *79*, 1631–1646.

33. Rao, Y.L., Ganaraja, B., Murlimanju, B., Joy, T., Krishnamurthy, A., and Agrawal, A. (2022). Hippocampus and its involvement in alzheimer's disease: a review. 3 Biotech *12*, 55.

34. Graff-Radford, J., Yong, K.X., Apostolova, L.G., Bouwman, F.H., Carrillo, M., Dickerson, B.C., Rabinovici, G.D., Schott, J.M., Jones, D.T., and Murray, M.E. (2021). New insights into atypical alzheimer's disease in the era of biomarkers. The Lancet Neurology *20*, 222–234.

35. Turk-Browne, N.B. (2019). The hippocampus as a visual area organized by space and time: A spatiotemporal similarity hypothesis. Vision Research *165*, 123–130.

36. Quiroga, R.Q., Nadasdy, Z., and Ben-Shaul, Y. (2004). Unsupervised spike detection and sorting with wavelets and superparamagnetic clustering. Neural Computation *16*, 1661–1687.